



Electrochemical Approaches for Material Conservation: Experimental and Theoretical Insights Using a Biopolymer

Mikitha Pais¹ · Padmalatha Rao¹

Received: 22 March 2020 / Revised: 22 March 2020 / Accepted: 13 August 2020 / Published online: 19 August 2020
© The Author(s) 2020

Abstract

Maltodextrin (MLD) is introduced as a novel, potent green inhibitor for the corrosion control of zinc in 0.1 sulfamic acid. The corrosion and inhibition studies were done by electrochemical techniques such as potentiodynamic polarisation measurements and electrochemical impedance spectroscopy technique. Conditions were optimised to get maximum inhibition efficiency by varying the concentration of the inhibitor in the temperature range of 303–323 K. Activation and thermodynamic parameters were evaluated and discussed in detail. Suitable mechanism was proposed for corrosion and inhibition process. Surface characterisation was done by SEM, EDX and AFM techniques before and after the addition of inhibitor. The density functional theory calculations were performed and compared with experimental observations. Results indicated that inhibition efficiency increased with the temperature and inhibitor concentration. Maximum inhibition efficiency was found to be 62.3% for the addition of 0.4 g L⁻¹ MLD. Theoretical calculations confirmed the experimental observations.

Keywords Carbohydrate polymer · Material conservation · Sulfamic acid · Electrochemical studies · Surface morphology · Theoretical calculations

1 Introduction

Zinc is currently ranked the third widely consumed nonferrous metal [1]. Zinc with its anticorrosive character has a wide range of applications in industrial and domestic sectors. It is mainly used in galvanising, where a thin layer of zinc is applied over steel or iron in order to protect it from corrosion [2, 3]. Although it is corrosion resistant, it undergoes severe corrosion in solutions which has the pH lower than 6 and higher than 12. Corrosion may occur slowly within the pH 6–12 [4].

In industries, aggressive mineral acids come in contact with the metal surface during surface treatment. With commonly preferred mineral acids like dilute hydrochloric acid, sulphuric acid etc., magnitude of corrosion is quite high

which results in considerable material loss. Sulfamic acid is an outstanding alternative for acid cleaning applications. Because of its dry form, it is easy to formulate, transport and handle. It forms soluble salts with most metals and is generally less corrosive to metals than the common inorganic acids. Absence of Cl⁻ ions eliminates the possibility of pitting corrosion and stress corrosion cracking. Presence of functional groups like –NH₂ and –OH helps in dissolving industrial deposits. Moreover it will not produce any harmful fumes like other mineral acids [5–7].

Even though a few reports are available in literature [8, 9] explaining the interaction of zinc with sulfamic acid, detailed investigation is yet to be explored. Realising the potency of sulfamic acid as safe, environmentally benign agent for pickling process, present work is carried out with 0.1 M sulfamic acid.

To prevent this considerable material loss acid environment, addition of inhibitors to the pickling bath is recommended. The unique property of these inhibitors is that they act without disturbing the original industrial process. Use of heterocyclic organic inhibitors is one of the most important methods to mitigate acid corrosion and numerous reports are available for the same [10–15]. But the toxic nature and high cost of some inorganic and organic inhibitors have paved a

Electronic supplementary material The online version of this article (<https://doi.org/10.1007/s40735-020-00412-4>) contains supplementary material, which is available to authorized users.

✉ Padmalatha Rao
padmalatha.rao@manipal.edu

¹ Department of Chemistry, Manipal Institute of Technology, MAHE, Manipal 576104, India

way in finding alternative inhibitors because the safety of human health and preservation of environment is of prime importance. In the present decade, research is more focused towards using nontoxic, eco-friendly, cheap and renewable source of materials.

Naturally occurring substances of both plant and animal origin have been found to satisfy this need. Even though synthetic polymers [16–20] have been reported as corrosion inhibitors for metals in various corrosive medium, non-biodegradability is always a problem. In this regard bio-polymers offer distinct advantages as green corrosion inhibitors.

Biologically derived polymers are the class of green inhibitors which are naturally available, eco-friendly, environmentally acceptable and nontoxic [21]. These polymers can effectively control the corrosion process of the metals because of the presence of multiple adsorption sites which has the tendency to easily form a complex with the metal surface. A few available literatures for using biopolymers as corrosion inhibitors are: sodium alginate for API X60 steel [22] pectin for mild steel [23] lignin for 3 different alloys like mild steel alloy, stainless steel alloy and aluminium zinc alloy [24] carboxymethyl starch for mild steel [25]. In continuation of our continuous effort towards corrosion mitigation and hence material conservation, using eco-friendly green inhibitors [26, 27] for various types of engineering materials [28, 29] we hereby introduce a novel carbohydrate polymer maltodextrin (MLD) for the corrosion control of zinc in sulfamic acid.

MLD is a carbohydrate polymer which is used primarily in foods and beverages as a thickener, sweetener and stabiliser. It is a relatively short-chain polymer and classified by dextrose equivalents (DE) ranging from 3 to 20 DE. MLD consists of D-glucose units connected in chains of variable length. The glucose units are primarily linked with $\alpha(1 \rightarrow 4)$ glycosidic bonds. It has a shelf life of about 4 years. MLD is safe, inexpensive and extremely water-soluble, and it is used widely as a food additive in a variety of products. MLD used for the present studies contains 16.5–19.5 DE. Structure of MLD is shown in Fig. S1.

2 Experimental: Materials and Methods

2.1 Preparation of Test Coupon and Inhibitor Solution

99.8% pure zinc was used for the study with the composition: 0.009% Al, 0.004% of Cr, 0.11% of Cu, 0.017% of Fe, 0.026% of Mg, 0.004% of Ni, 0.006% of Pb, 0.005% of Sn and 99.8% of zinc. A cylindrical metal zinc rod with a surface area of 0.95 cm^2 was sealed with resin material. Material abrasion was first done with different grades of emery papers (220–1500) and then with disc polisher using

lavigated alumina. The material was washed, dried and used for studies.

Sulfamic acid (Sigma-Aldrich) was 99% pure. Fresh solution of 0.1 M was prepared by dissolving calculated amount of the crystals in double distilled water. Inhibitor solution was prepared by dissolving required weight of MLD (Sigma-Aldrich, Molecular weight 2774.7 Da) in 0.1 M $\text{NH}_2\text{SO}_3\text{H}$. The inhibitor concentration used was in the range of 25–400 ppm. The experiments were conducted at the temperature range of 303–323 K, in a thermostat calibrated up to $\pm 0.5 \text{ }^\circ\text{C}$ under unstirred condition.

2.2 Electrochemical Measurements

The corrosion rate measurements were taken by electrochemical methods like potentiodynamic polarisation (PDP) method and electrochemical impedance spectroscopy (EIS) method. Corrosion studies of zinc were carried out by using electrochemical work station (CH600 D—series US model with CH instrument with beta software). The electrochemical cell used was a conventional three-electrode compartment pyrex glass vessel comprising a reference electrode that is the saturated calomel electrode and platinum as auxiliary electrode the metal zinc is the working electrode. The potential values will be recorded with respect to the reference saturated calomel electrode. The potentiodynamic polarisation (PDP) studies and the EIS studies were carried out by the methods reported in literature [30].

2.3 Surface Morphology, Elemental Composition and Surface Roughness Studies

Surface studies were done by immersing the metal in 0.1 M $\text{NH}_2\text{SO}_3\text{H}$ for 2 h without and with the addition of the MLD (0.4 g L^{-1}). Surface morphology of zinc was carried out by using analytical scanning electron microscope (SEM) (JEOL JSM–6380L) in the magnification of 500 \times . Elemental mapping was done by using energy-dispersive X-Ray (EDX) analysis. Surface roughness was ascertained by atomic force microscopic (AFM) technique, by using 1B342 innova model.

2.4 Theoretical Studies

The quantum chemical calculations were performed on the studied inhibitor using the density functional theory (DFT) method by Maestro Material Science, Schrodinger software. The DFT calculations were performed using the hybrid functional with the correlation functional (B3LYP) and 6-31G as the basis set. The frontier molecular orbital (FMO) energies, i.e. the energy of the highest occupied molecular orbital (E_{HOMO}) and the energy of the lowest unoccupied molecular orbital (E_{LUMO}) and Mullikan's charge population were

evaluated. Other alternate parameters were obtained from theoretical studies [31–33].

3 Results and Discussion

3.1 Potentiodynamic Polarisation (PDP) Studies

The potentiodynamic polarisation curve for 0.1 M $\text{NH}_2\text{SO}_3\text{H}$ is shown in Fig. 1. and results are tabulated in Table 1. From the obtained plots, the electrochemical parameters like corrosion current density (i_{corr}), Tafel slop, corrosion potential (E_{corr}) were obtained. The percentage inhibition efficiency of the inhibitor in the corrosive medium was then calculated using Eq. (1).

$$IE(\%) = \frac{i_{\text{corr}} - i_{\text{corr(inh)}}}{i_{\text{corr}}} \times 100 \quad (1)$$

where i_{corr} : corrosion current density (mA cm^{-2}) in the absence of inhibitor. $i_{\text{corr(inh)}}$: corrosion current density in presence of inhibitor.

From Table 1 it is evident that corrosion current density and corrosion rate decreased with the increase in the concentration of MLD and hence the inhibition efficiency increased. The increased adsorption of the inhibitor molecule on the metal surface was responsible for the increase in inhibition efficiency. The adsorbed inhibitor molecule forms a protective barrier at the electrode/electrolyte interface leading to the isolation of metal from the corrosive environment thereby decreasing the corrosion rate [34].

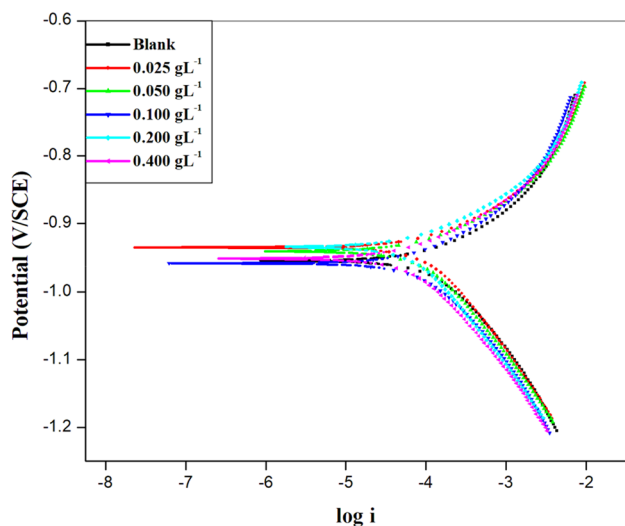


Fig. 1 Potentiodynamic polarisation plot for the corrosion control of zinc containing various concentrations of MLD in 0.1 M $\text{NH}_2\text{SO}_3\text{H}$ at 313 K

The PDP plot is characterised by cathodic and anodic tafel curves. Metal dissolution is represented by the anodic curve while the cathodic curve represents hydrogen evolution process. It was observed that with the addition of the inhibitor there was no change in the shape of both the anodic and cathodic tafel curve. The added inhibitor did not bring any remarkable change in both the cathodic and anodic slope. This suggested that mechanism of both anodic and cathodic reactions remain almost unaffected after the addition of inhibitor. The inhibitor molecules adsorb on the zinc surface and block the available reaction sites on the metal surface and brings down the corrosion rate without altering the mechanism [35, 36].

Standard electrode potential of Zinc is -760 V. During corrosion and inhibition process the corrosion potential was shifted to a remarkable extent. As per the reported literature, this type of observation can be made under two situations. One possible reason is the passivity of the metal and another could be presence of oxidising agent in the corrosive. In the present study, observed shift of around -960 V could be attributed to the presence of free oxygen in the corrosive environment [37].

As per the reported literature [38], if the shift in the corrosion potential (E_{corr}) is more than ± 85 mV, the inhibitor can be distinctly considered as anodic or cathodic or else it can be regarded as mixed inhibitor. In the present study the observed difference is less than $+36$ mV. It is slightly towards the positive side. It can be concluded that inhibitor acts as mixed inhibitor with more control on the metal dissolution.

Inhibition efficiency of MLD increased with increase in temperature. This is suggestive of chemical adsorption of inhibitor onto the metal surface [39]. At 323 K a maximum efficiency of 62.3% was observed for the addition of 0.4 g L^{-1} of inhibitor in 0.1 M sulfamic acid.

3.2 Electrochemical Impedance Spectroscopy (EIS) Studies

Nyquist plots obtained at 318 K for the corrosion control of zinc in 0.1 M $\text{NH}_2\text{SO}_3\text{H}$ in the absence and presence of various concentrations of MLD are shown in Fig. 2. Similar plots were obtained even at other temperatures. Shape of the Nyquist plots agrees well with that reported in the literature for the corrosion of zinc in various other acid medium [40, 41].

The semicircle Nyquist plot of 0.1 M acid showed a single loop, the capacitive loop in the high frequency (HF) region. High-frequency capacitive loop is indicative of charge transfer resistance of zinc in the absence and presence of inhibitor. In the absence of inhibitor, diameter of the semicircle is small, indicating least resistance of the metal for corrosion. The diameter of the capacitive loop increased with the increase in

Table 1 Results of potentiodynamic polarisation measurements for the corrosion control of zinc containing various concentrations of MLD in 0.1 M NH₂SO₃H

| Temp (K) | [MLD] (g L ⁻¹) | E_{corr} vs SCE (mV) | i_{corr} (10 ⁻⁵ A cm ⁻²) | $-\beta_c$ (V dec ⁻¹) | β_a (V dec ⁻¹) | CR (mpy) | IE (%) |
|----------|----------------------------|-------------------------------|--|-----------------------------------|----------------------------------|----------|--------|
| 303 | Blank | -935 | 06.35 | 7.48 | 12.44 | 39.47 | - |
| | 0.025 | -952 | 05.80 | 8.44 | 12.92 | 37.44 | 08.6 |
| | 0.050 | -943 | 05.52 | 7.67 | 12.82 | 34.31 | 13.0 |
| | 0.100 | -971 | 05.07 | 6.75 | 12.00 | 31.54 | 20.0 |
| | 0.200 | -936 | 04.58 | 7.14 | 12.93 | 28.46 | 27.8 |
| | 0.400 | -951 | 04.02 | 7.53 | 12.92 | 27.69 | 36.6 |
| 308 | Blank | -942 | 10.85 | 7.23 | 10.68 | 67.41 | - |
| | 0.025 | -963 | 09.55 | 7.82 | 10.16 | 61.84 | 11.9 |
| | 0.050 | -950 | 08.97 | 7.78 | 11.02 | 55.76 | 17.2 |
| | 0.100 | -944 | 07.76 | 7.39 | 11.36 | 48.24 | 28.4 |
| | 0.200 | -941 | 06.96 | 7.36 | 11.85 | 43.25 | 35.8 |
| | 0.400 | -931 | 05.84 | 7.06 | 12.44 | 36.32 | 46.1 |
| 313 | Blank | -954 | 15.70 | 7.41 | 08.99 | 97.52 | - |
| | 0.025 | -935 | 13.47 | 6.93 | 10.01 | 83.65 | 14.2 |
| | 0.050 | -941 | 11.59 | 7.19 | 10.54 | 71.95 | 26.1 |
| | 0.100 | -958 | 10.40 | 7.68 | 09.81 | 64.62 | 33.7 |
| | 0.200 | -934 | 09.08 | 6.95 | 10.98 | 56.41 | 42.1 |
| | 0.400 | -951 | 07.38 | 7.66 | 11.61 | 45.89 | 52.9 |
| 318 | Blank | -942 | 23.52 | 6.42 | 08.81 | 146.1 | - |
| | 0.025 | -938 | 19.83 | 6.82 | 08.79 | 123.1 | 15.6 |
| | 0.050 | -949 | 16.05 | 6.89 | 09.07 | 99.70 | 31.7 |
| | 0.100 | -941 | 13.96 | 6.76 | 09.40 | 86.67 | 40.6 |
| | 0.200 | -955 | 11.62 | 7.67 | 09.72 | 72.17 | 50.5 |
| | 0.400 | -952 | 09.87 | 7.65 | 10.94 | 56.37 | 58.0 |
| 323 | Blank | -945 | 33.36 | 6.05 | 07.98 | 207.2 | - |
| | 0.025 | -948 | 27.57 | 6.45 | 08.00 | 170.9 | 17.3 |
| | 0.050 | -946 | 21.29 | 6.70 | 08.57 | 132.2 | 36.1 |
| | 0.100 | -950 | 17.82 | 6.94 | 09.37 | 110.6 | 46.5 |
| | 0.200 | -955 | 14.75 | 7.42 | 09.05 | 91.61 | 55.7 |
| | 0.400 | -950 | 12.55 | 7.56 | 09.64 | 77.93 | 62.3 |

the concentration of the MLD. This suggested that decrease in corrosion rate occurred by the hindrance of charge transfer process due to the adsorption of MLD on the zinc surface.

Figure 3 represents the impedance spectra for Nyquist plots by fitting the experimental data to the equivalent circuit model, using ZSimpWin software 3.1. The equivalent circuit for zinc in 0.1 M acid consisted of the following elements: solution resistance (R_1), charge transfer resistance (R_3), a constant phase element (Q), which is parallel to the capacitance C and also parallel to the series of resistor R_2 and R_3 (Fig. 3a, b).

Equations (2) and (3) were used to calculate the polarisation resistance (R_p) and double layer capacitance (C_{dl}) from the values obtained from circuit fitment.

$$R_p = R_1 + R_2 + R_3 \quad (2)$$

$$C_{dl} = \frac{1}{2\pi f \max R_p} \quad (3)$$

f_{\max} is the frequency at which the imaginary component of impedance is maximum.

The values of electrochemical impedance parameters obtained from fitting the experimental data to the used equivalent model are presented in Table 2.

From Table 2 it is evident that with the increase in concentration of MLD, the polarisation resistance increased and the double layer capacitance decreased. The increased R_p values are due to resistance to corrosion attack offered by the added inhibitor and decrease in the C_{dl} value is because of the decrease in the dielectric constant and increase in the thickness of the double layer at metal/electrolyte interface. The inhibition efficiency obtained from the PDP measurements was in good agreement with that obtained from the EIS studies.

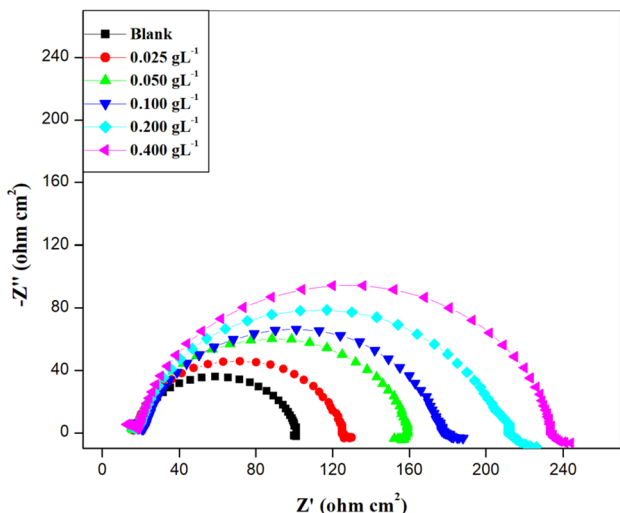


Fig. 2 Nyquist plot for the corrosion control of zinc in the absence and presence of various concentrations of MLD in 0.1 M NH₂SO₃H at 313 K

3.3 Effect of Temperature

The study of effect of temperature on the corrosion process is helpful in calculating the activation parameters such as energy of activation (E_a), enthalpy of activation (ΔH_a) and entropy (ΔS_a) of activation. The E_a was calculated using Arrhenius law Eq. (4).

$$\ln(CR) = B - \frac{E_a}{RT} \tag{4}$$

where B (Arrhenius constant) depends on the metal type and R is universal gas constant (8.314 J K⁻¹ mol⁻¹), T is the temperature. The plot of ln(CR) versus (1/T) (Fig. S2a) gave a straight line with a slope = $-E_a/R$, from which E_a for the corrosion and the inhibition process was calculated.

The transition state equation was used to calculate ΔH_a and ΔS_a for the dissolution of metal and its inhibition process. The transition state Eq. (5) is given below,

$$\ln \frac{CR}{T} = \ln \frac{R}{Nh} + \frac{\Delta S_a}{R} - \frac{\Delta H_a}{RT} \tag{5}$$

where h is planks constant (6.626×10^{-34} m² kg s⁻¹), N is Avogadro’s number (6.023×10^{23}), R is universal gas constant [42]. The plot of ln (CR/T) versus 1/T (Fig.S2b) gave a straight line with slope = $-\frac{\Delta H_a}{R}$; and the intercept = $(\ln(R/Nh) + \frac{\Delta S_a}{R})$. From this the values of ΔH_a and ΔS_a were calculated.

Activation parameters for the corrosion of zinc in 0.1 M NH₂SO₃H containing different concentrations of MLD are tabulated in (Table S1).

Energy of activation (E_a) values of the inhibited solutions was comparatively lesser to that of uninhibited solution. MLD molecule has oxygen as heteroatom; it can form easily coordinate bond with the zinc surface. The adsorbed molecule on the metal surface blocks the process of charge transfer during the corrosion of zinc. This leads to the decrease in energy of activation [39, 43, 44]. The positive signs of ΔH_a reflect the endothermic process of zinc dissolution [45]. The decreased value of ΔS_{ads} with increasing inhibitor concentrations reveals that a decrease in disordering takes place on going from reactant to the activated complex. This behaviour can be explained as a result of the replacement process of water molecules during adsorption of MLD molecules onto the zinc surface [46].

3.4 Adsorption Considerations

The surface coverage (θ) values were obtained from the relation (6)

$$\theta = \frac{\%IE}{100} \tag{6}$$

These values were fitted into various adsorption isotherms. The experimental data of corrosion of zinc in 0.1 M NH₂SO₃H with MLD best fitted into Langmuir adsorption isotherm

Langmuir adsorption model is given by Eq. (7)

$$\frac{C}{\theta} = \frac{1}{K} + C \tag{7}$$

Langmuir adsorption isotherm for the adsorption of MLD is shown in (Fig. S3). Plot of C/θ versus C was a straight line

Fig. 3 a Stimulated circuit fitted to the obtained EIS data for 0.1 M NH₂SO₃H. **b** Circuit used to fit the experimental EIS data

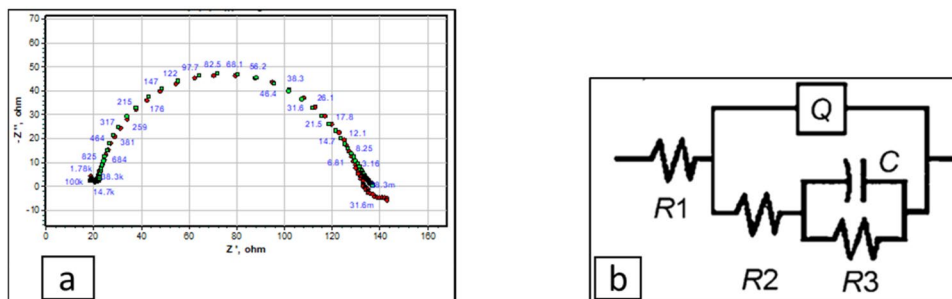


Table 2 Results of EIS measurements for the corrosion control of zinc containing various concentrations of maltodextrin in 0.1 M NH₂SO₃H

| Temp (K) | [MLD] (g L ⁻¹) | R _p (Ω cm ²) | C _{dl} (μ F cm ⁻²) | IE (%) |
|----------|----------------------------|-------------------------------------|---|--------|
| 303 | Blank | 217.3 | 9.01 | – |
| | 0.025 | 233.3 | 8.21 | 06.8 |
| | 0.050 | 247.1 | 7.47 | 12.0 |
| | 0.100 | 275.0 | 5.89 | 20.3 |
| | 0.200 | 295.5 | 5.34 | 26.4 |
| | 0.400 | 348.5 | 4.08 | 37.6 |
| 308 | Blank | 146.7 | 16.5 | – |
| | 0.025 | 169.1 | 15.6 | 13.2 |
| | 0.050 | 175.3 | 12.1 | 16.3 |
| | 0.100 | 207.6 | 8.86 | 29.3 |
| | 0.200 | 226.2 | 7.10 | 35.1 |
| | 0.400 | 273.1 | 4.62 | 46.2 |
| 313 | Blank | 100.9 | 44.8 | – |
| | 0.025 | 114.9 | 20.5 | 12.1 |
| | 0.050 | 138.2 | 16.4 | 27.0 |
| | 0.100 | 151.5 | 14.8 | 33.4 |
| | 0.200 | 180.0 | 11.4 | 43.9 |
| | 0.400 | 216.2 | 7.87 | 53.3 |
| 318 | Blank | 81.21 | 67.9 | – |
| | 0.025 | 97.18 | 32.7 | 16.4 |
| | 0.050 | 117.6 | 26.5 | 30.9 |
| | 0.100 | 137.2 | 21.6 | 40.8 |
| | 0.200 | 169.0 | 15.1 | 51.9 |
| | 0.400 | 192.1 | 8.95 | 57.7 |
| 323 | Blank | 68.63 | 98.1 | – |
| | 0.025 | 85.23 | 47.1 | 19.4 |
| | 0.050 | 104.5 | 37.3 | 34.3 |
| | 0.100 | 122.6 | 29.9 | 44.0 |
| | 0.200 | 151.7 | 20.2 | 54.7 |
| | 0.400 | 176.4 | 14.9 | 61.1 |

with an average correlation coefficient (R^2) equal to 0.9998, which indicated the validity of adsorption of MLD through Langmuir adsorption isotherm [47].

From the intercept of above adsorption isotherms, adsorption equilibrium constant (K) was obtained, which is related to standard free energy of adsorption (ΔG°) by Eq. (8)

$$\Delta G^\circ_{\text{ads}} = -RT \ln K \quad (8)$$

where R is the universal gas constant (8.314 J mol⁻¹ K⁻¹), T is the absolute temperature. It is well known that the unit for $\Delta G^\circ_{\text{ads}}$ is J mol⁻¹. Since the unit for the term RT is also J mol⁻¹, adsorption equilibrium constant (K) must be dimensionless. However, by taking units of concentration of inhibitor and water same, K obtained from Eq. (7) will be in the dimension of Lg⁻¹. In such situation, K can

be easily recalculated as dimensionless by multiplying it by 1000 (number of grams of water per litre of solution). Accordingly, the correct $\Delta G^\circ_{\text{ads}}$ value can be obtained from Eq. (9) [48],

$$\Delta G^\circ_{\text{ads}} = -RT \ln(1000K) \quad (9)$$

The standard enthalpy (ΔH°) of adsorption and standard entropy of adsorption (ΔS°) was calculated by plotting ΔG° versus T (Fig. S4.) using Eq. (10). The results are tabulated in Table S2.

$$\Delta G^\circ_{\text{ads}} = \Delta H^\circ_{\text{ads}} - T\Delta S^\circ_{\text{ads}} \quad (10)$$

Negative values of standard free energy of adsorption ($\Delta G^\circ_{\text{ads}}$) suggested the spontaneity of the adsorption of MLD on metal surface [49, 50]. Calculated values $\Delta G^\circ_{\text{ads}}$ were in the range of -23 kJ mol⁻¹. These values which are greater than -20 kJ mol⁻¹, indicated that the adsorption of inhibitor involves both physisorption and chemisorption. However, an exothermic adsorption process signifies either physical adsorption or chemical adsorption, while the endothermic process is attributable unequivocally to chemical adsorption [10, 51, 52]. In the present investigation standard enthalpy of adsorption was positive and is equal to 47.07 kJ mol⁻¹. This clearly demonstrated the chemical adsorption of inhibitor onto the metal surface. Further it is supported by the fact that, inhibition efficiency increased with increase in temperature [53]. $\Delta S^\circ_{\text{ads}}$ positive values reflect the increase in the solvent entropy as disorder occurs at the metal/solution interface. This is attributed to the displacement of H₂O molecules by MLD molecules from the metal surface [54].

3.5 Surface Morphology Studies

3.5.1 Scanning Electron Microscopy (SEM) Analysis

Figure 4a shows the freshly polished zinc surface. It is very smooth except few scratches, which could be due to the polishing. Figure 4b shows the metal surface in contact with 0.1 M NH₂SO₃H for 2 h. Zinc is expected to undergo severe corrosion in the pH below 6 [55, 56]. Likewise, the surface of the corroded sample has become highly uneven due to the dissolution of metal and deposition of corrosion product. The formation of these cavities could be due to the detachment of corrosion product from the metal. Addition of 0.4 g L⁻¹ MLD showed remarkable change in the surface of the metal (Fig. 4c). The added inhibitor was able to cover almost all the cavities present on the surface forming a barrier between the metal and the medium preventing further corrosion.

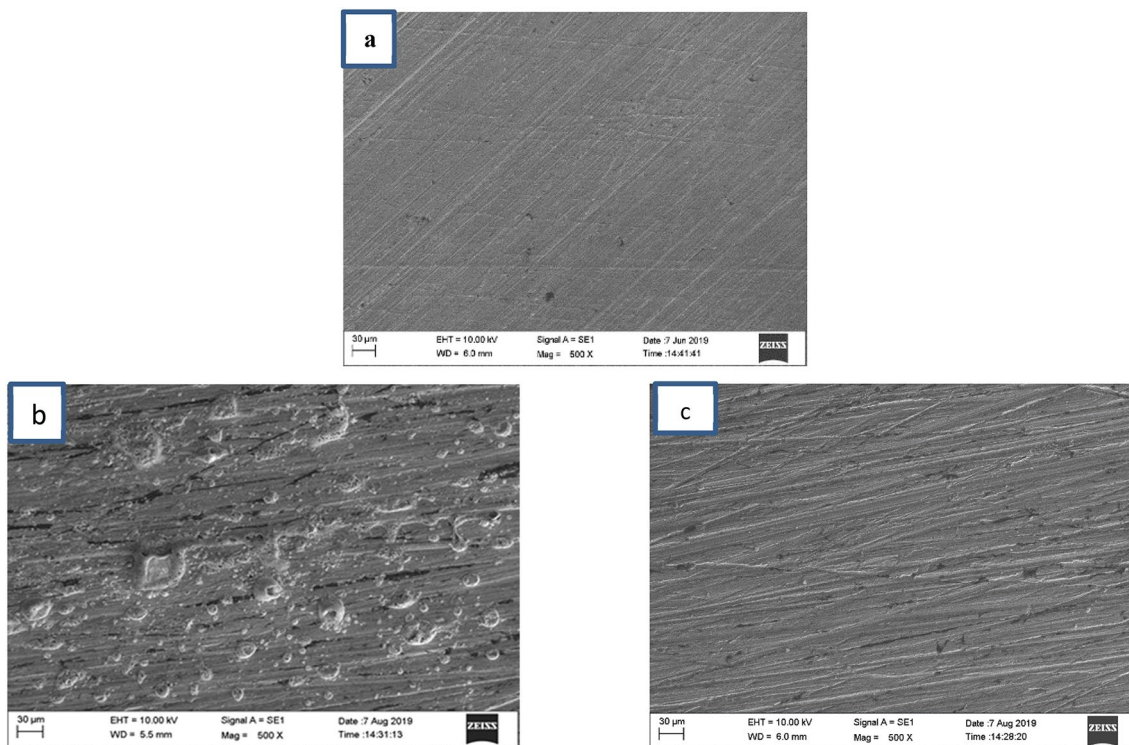


Fig. 4 **a** Freshly polished zinc metal, **b** zinc metal + 0.1 M $\text{NH}_2\text{SO}_3\text{H}$, **c** zinc metal + 0.1 M $\text{NH}_2\text{SO}_3\text{H}$ + 0.4 g L^{-1} MLD

3.5.2 EDX Analysis

It is evident from the Table S3 that % composition of oxygen has been increased in the corroded sample. This shows that the corrosion of metal has taken place and a metal oxide layer is formed on the metal surface. The addition of 0.4 g L^{-1} MLD increased the % composition of carbon (12%) on the metal surface. This is because the backbone of MLD is mainly composed of carbon atoms. This reaffirmed the adsorption of MLD on the surface of the metal which effectively decreases the extent of corrosion.

3.5.3 AFM Analysis

The 3-dimensional images of zinc surface for the freshly polished (Fig. 5a), specimen immersed in 0.1 M $\text{NH}_2\text{SO}_3\text{H}$ (Fig. 5b) and specimen immersed in 0.1 M $\text{NH}_2\text{SO}_3\text{H}$ along with the 0.4 g L^{-1} MLD (Fig. 5c.) are shown, respectively.

Table S4 shows the R_a , R_q and R_{max} values obtained from AFM analysis. The values of R_a , R_q and R_{max} of the specimen in the inhibited solutions (117 nm, 146 nm, 1042 nm) were much lesser than the specimen in the absence of the inhibitor (122 nm, 158 nm, 1428 nm). This clearly suggested that the MLD adsorbed onto the surface of the metal [57, 58].

3.6 Mechanism of Corrosion and Inhibition Process

The adsorption of inhibitor on a metal surface depends on their chemical structure, the distribution charge in the molecule, the aggressive medium and the topography of the metal surface. The initial mechanism in any corrosion inhibition is the adsorption of the inhibitor on the surface of the metal. Inhibitors adsorb on to the metal surface from aqueous solution, where they block the active sites of metal which are susceptible to corrosion. The strong adsorption of the inhibitor onto the zinc surface was due to the presence of large number of oxygen atoms in the inhibitor molecule. This results in the strong bonding between the metal and the inhibitor [59].

The interaction between the metal and the inhibitor has predominantly obeyed chemisorption as suggested by the thermodynamic parameters. The presence of oxygen in the inhibitor molecule having lone pair of electrons has promoted chemical adsorption onto the metal surface. This process is accompanied by the replacement of water molecules which were adsorbed onto the metal surface. As MLD belongs to the category of biopolymers it is obvious that the molecule is bigger in size and hence it is capable of covering both cathodic and anodic area due to Umbrella effect. Thus, it acts as a mixed inhibitor. This explanation

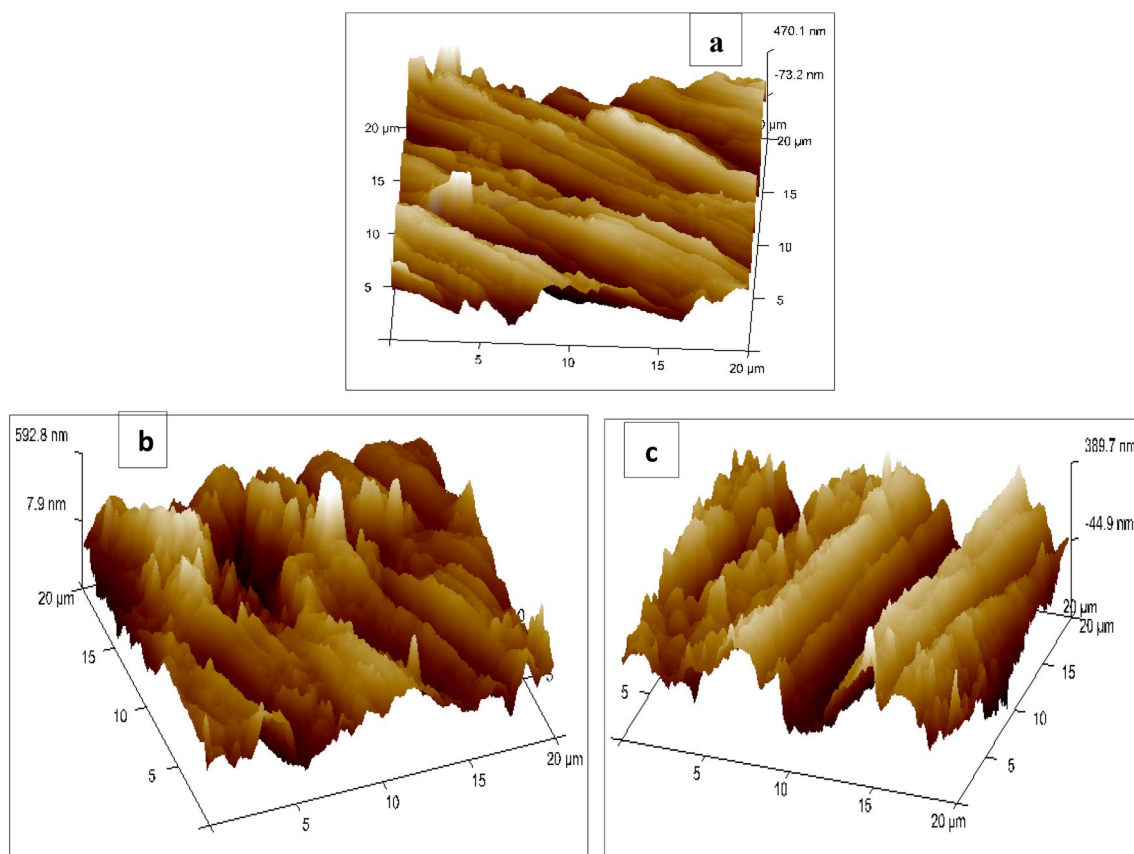


Fig. 5 AFM spectra of **a** freshly polished zinc, **b** zinc + 0.1 M $\text{NH}_2\text{SO}_3\text{H}$, **c** zinc + $\text{NH}_2\text{SO}_3\text{H}$ + 0.4 g L^{-1} MLD

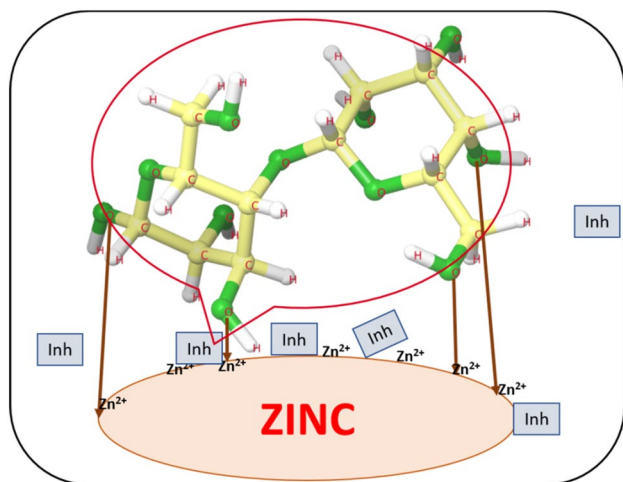


Fig. 6 Representation of chemical adsorption of MLD over zinc

agrees very well with the observation of potentiodynamic polarisation method. Figure 6 shows the pictorial representation of adsorption of the inhibitor.

3.7 Quantum Chemical Calculations

The inhibition action of MLD on the metal zinc in 0.1 M $\text{NH}_2\text{SO}_3\text{H}$ medium can be explained by quantum mechanical studies using DFT method. Corrosion inhibition capacity of the molecule largely depends upon its electron releasing capacity and its adsorption power. DFT method enables the calculation of various chemical functional parameters like energy of HOMO, LUMO, energy gap (ΔE), dipole moment (μ), Mulliken charges, etc.,

Optimised structure of MLD is shown in Fig. 7a. The optimised geometry of frontier molecular orbital of HOMO and LUMO are shown in Fig. 7b, c. The distribution of electron density is localised both on HOMO and LUMO; this confirms that the both the electron accepting and donating centres are present in MLD.

Various quantum mechanical parameters for the MLD are tabulated in Table 3 and discussed in detail in the following section.

According to the frontier molecular orbital theory, the energy gap ($\Delta E = E_{\text{LUMO}} - E_{\text{HOMO}}$) is related to the inhibition efficiency of inhibitor [60]. Adsorption of MLD onto the zinc surface can occur through donor acceptor

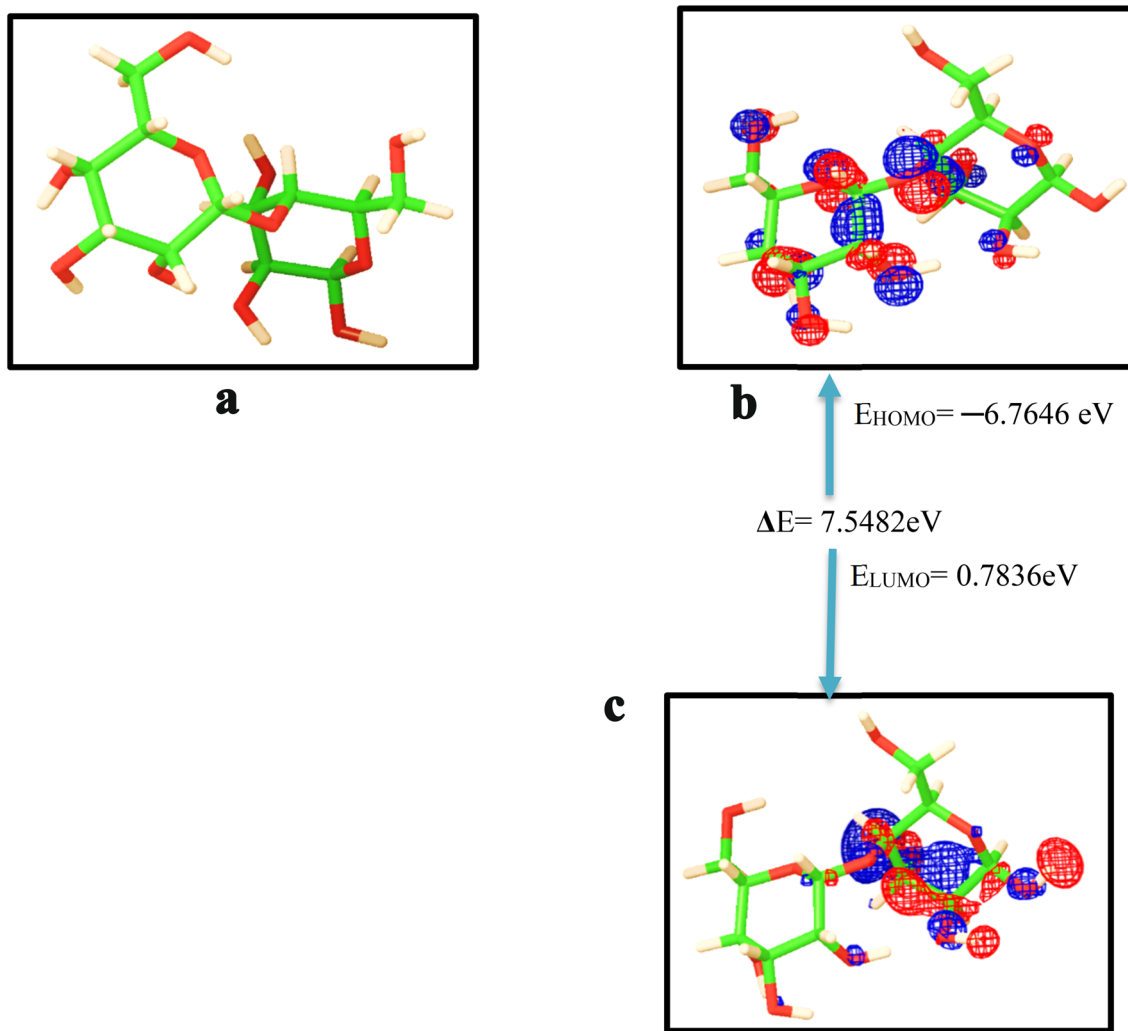


Fig. 7 a Optimised structure of MLD, b HOMO, c LUMO

Table 3 Quantum chemical parameters of the neutral MLD

| MLD | E_{HOMO} | E_{LUMO} | ΔE | χ | η | σ | ω | ϵ | ΔN | μ |
|---------|-------------------|-------------------|------------|--------|--------|----------|----------|------------|------------|-------|
| Neutral | -6.7646 | 0.7836 | 7.5482 | 2.9905 | 3.7741 | 0.2649 | 0.5923 | 1.688 | 0.174 | 2.968 |

All energy values are in eV, μ in Debye, σ is in eV^{-1}

interactions with the biopolymer which can donate electrons. The higher value of E_{HOMO} suggests higher capability of inhibitor molecule to donate the electrons to form coordinate bond with zinc metal. E_{LUMO} value being smaller reflects the electron acceptance tendency of inhibitor. The energy gap ($\Delta E = 7.5482 \text{ eV}$) demonstrates the inherent electron donating ability and measures the interaction of the inhibitor molecule with the zinc surface. It has been reported that low values of ΔE will provide good inhibition efficiency, because the energy for removing an electron from the last occupied orbital will be low [61]. The HOMO is concentrated in the zone to the oxygen

(Fig. 6b), which is attributed to the presence of a lone pair of electrons in the oxygen atom of MLD. So, the preferred active sites for donating electrons in MLD are located in the regions around the oxygen atoms. The dipole moment (μ) value of MLD is 2.9689 Debye which is higher than the dipole moment of water (1.88 Debye), indicating that there is a strong dipole–dipole interaction between the inhibitor molecule and the zinc surface. This implies that the displacement of the water molecules from the metal surface is favourable and MLD gets chemically adsorbed onto the metal surface [62].

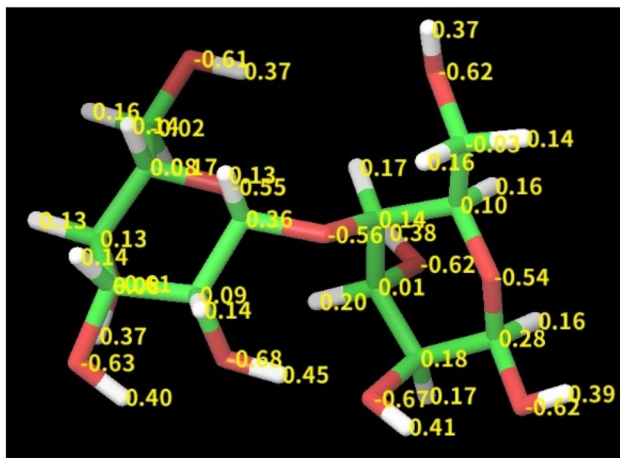


Fig. 8 Mullikan charge population

Computed values of electronegativity (χ) and chemical hardness (η) enable the evaluation of fraction of electron transferred (ΔN) [63–65] using the relation (11)

$$\Delta N = \frac{\phi_{Zn} - \chi_{inh}}{2\eta_{inh}} \tag{11}$$

where ϕ_{Zn} is the work function of the Zn which is equal to 4.31 eV. As per the reported literature [66] ΔN value less than 3.6 suggests the electron releasing ability of the inhibitor molecule. Calculated value of ΔN value for MLD is 0.174, which clearly suggests its electron releasing ability thereby confirming the formation the physical barrier on the metal surface. The absolute electronegativity (χ) and global electrophilicity (ω) of MLD were 2.9905 and 0.5923 which indicated the stability and reactivity of inhibitor molecule. Mullikan charge population for MLD is shown in Fig. 8.

Mullikan charge density values provide useful information in locating high electron density region of the inhibitor molecule [67, 68]. Higher the electron density on the heteroatom, stronger will be the coordinate bond between inhibitor and metal [69]. Careful observation of Figure shows accumulation of excess of negative charges on the oxygen atom of –OH group. This facilitates the barrier between the metal and the corrosive and brings down the corrosion rate. Table 4 shows the Mullikan charge population on heteroatoms of MLD.

4 Conclusions

1. A maximum inhibition efficiency of 62.3% was obtained for 0.4 g L⁻¹ inhibitor concentration at 323 K.
2. MLD acted as a mixed inhibitor, underwent chemisorption and obeyed Langmuir adsorption isotherm.

Table 4 Mullikan charges on heteroatoms of MLD

| | | | | | | | | | | | |
|-----------------|-------|-------|--------|--------|--------|--------|--------|--------|--------|--------|--------|
| Heteroatom | O (7) | O (8) | O (11) | O (15) | O (16) | O (17) | O (19) | O (20) | O (21) | O (22) | O (23) |
| Mullikan charge | -0.54 | -0.55 | -0.53 | -0.61 | -0.66 | -0.61 | -0.62 | -0.68 | -0.62 | -0.61 | -0.61 |

3. Surface morphology studies using SEM, EDX and AFM confirmed the adsorption of MLD.
4. Quantum chemical calculations supported all the experimental observations.
5. MLD emerged as an eco-friendly, nontoxic, bio-degradable green inhibitor with environment and economic benefits.

Acknowledgements Ms. Mikitha Pais is grateful to MAHE, for the fellowship. Both the authors are thankful to Department of Chemistry, MIT MAHE for lab facilities, and Department of Mechanical Engineering, MAHE, Central Instrumentation Facilities MAHE for extending required facilities.

Funding This study was funded by Manipal University (Grant No. MAHE/DREG/PhD/IMF/2019). Open access funding provided by Manipal Academy of Higher Education, Manipal.

Compliance with Ethical Standards

Conflict of interest We state that there is no conflict of interest.

Open Access This article is licensed under a Creative Commons Attribution 4.0 International License, which permits use, sharing, adaptation, distribution and reproduction in any medium or format, as long as you give appropriate credit to the original author(s) and the source, provide a link to the Creative Commons licence, and indicate if changes were made. The images or other third party material in this article are included in the article's Creative Commons licence, unless indicated otherwise in a credit line to the material. If material is not included in the article's Creative Commons licence and your intended use is not permitted by statutory regulation or exceeds the permitted use, you will need to obtain permission directly from the copyright holder. To view a copy of this licence, visit <http://creativecommons.org/licenses/by/4.0/>.

References

1. Sabnavis M, Economist C (2018) Zinc Industry : the unsung metal of the economy
2. Hebbar N, Praveen BM, Prasanna BM, Venkatesha TV (2015) Anticorrosion potential of a pharmaceutical intermediate Floctafene for zinc in 0.1 M HCl solution. *Int J Ind Chem* 6:221–231. <https://doi.org/10.1007/s40090-015-0049-5>
3. Eddy NO, Odoemelam SA, Ogoko EC, Ita BI (2010) Inhibition of the corrosion of zinc in 0.01 - 0.04 M H₂SO₄ by erythromycin. *Port Electrochim Acta* 28:15–26. <https://doi.org/10.4152/pea.201001015>
4. Guruprasad AM, Sachin HP, Swetha GA, Prasanna BM (2019) Adsorption and inhibitive properties of seroquel drug for the corrosion of zinc in 0.1 M hydrochloric acid solution. *Int J Ind Chem* 10:17–30. <https://doi.org/10.1007/s40090-018-0168-x>
5. Morad MS (2008) Corrosion inhibition of mild steel in sulfamic acid solution by S-containing amino acids. *J Appl Electrochem* 38:1509–1518. <https://doi.org/10.1007/s10800-008-9595-2>
6. Hermas AA, Morad MS (2008) A comparative study on the corrosion behaviour of 304 austenitic stainless steel in sulfamic and sulfuric acid solutions. *Corros Sci* 50:2710–2717. <https://doi.org/10.1016/j.corsci.2008.06.029>
7. Motamedi M, Tehrani-Bagha AR, Mahdavian M (2013) Effect of aging time on corrosion inhibition of cationic surfactant on mild steel in sulfamic acid cleaning solution. *Corros Sci* 70:46–54. <https://doi.org/10.1016/j.corsci.2013.01.007>
8. Vashi RT, Champaneri VA (1997) Toluidines as corrosion inhibitors for zinc in sulphamic acid. *Indian J Chem Technol* 4:180–184
9. Vashi RT, Champaneri VA (1998) Inhibition of corrosion of zinc in sulphamic acid. *Asian J Chem* 10:280–286
10. El-Sherbini EEF, Wahaab SMA, Deyab M (2005) Ethoxylated fatty acids as inhibitors for the corrosion of zinc in acid media. *Mater Chem Phys* 89:183–191. <https://doi.org/10.1016/j.matchemphys.2003.09.055>
11. Morad MS (1999) Inhibition of phosphoric acid corrosion of zinc by organic onium compounds and their adsorption characteristics. *J Appl Electrochem* 29:619–626. <https://doi.org/10.1023/A:1026445521937>
12. Talati JD, Desai MN, Shah NK (2005) Meta-Substituted aniline-N-salicylidenes as corrosion inhibitors of zinc in sulphuric acid. *Mater Chem Phys* 93:54–64. <https://doi.org/10.1016/j.matchemphys.2005.02.004>
13. Shylesha BS, Venkatesha TV, Praveen BM (2011) New electroactive compounds as corrosion inhibitors for zinc in acidic medium. *Adv Appl Sci Res* 2:333–341
14. Fouda AS, Rashwan S, Emam A, El-Morsy FE (2018) Corrosion inhibition of zinc in acid medium using some novel organic compounds. *Int J Electrochem Sci* 13:3719–3744. <https://doi.org/10.20964/2018.04.23>
15. Vashi RT, Desai K (2013) Aniline as corrosion inhibitor for zinc in hydrochloric acid. *Chem Sci Trans* 2:670–676. <https://doi.org/10.7598/cst2013.423>
16. Dwivedi A, Bharti PK, Shukla SK (2018) Interaction of water soluble polyacrylic acid with mild steel/hydrochloric acid interface. *IOP Conf Ser Mater Sci Eng* 404:012044. <https://doi.org/10.1088/1757-899X/404/1/012044>
17. Harabor I, Nechifor G, Branzoi V et al (2016) Investigation of some organic polymers as corrosion inhibitors on carbon steel in cooling water systems. *Univ Politeh Buchar Sci Bull Series B-Chem Mater Sci* 78(3):145–160
18. Sekine I, Sanbongi M, Hagiuda H et al (1992) Corrosion inhibition of mild steel by cationic and anionic polymers in cooling water system. *J Electrochem Soc* 139:3167–3173. <https://doi.org/10.1149/1.2069050>
19. Tsoeunyane MG, Makhatha ME, Arotiba OA (2019) Corrosion inhibition of mild steel by poly(butylene succinate)-L-histidine extended with 1,6-diisocyanatohexane polymer composite in 1 M HCl. *Int J Corros*. <https://doi.org/10.1155/2019/7406409>
20. Azzam EMS, El-Salam HMA, Mohamed RA et al (2018) Control the corrosion of mild steel using synthesized polymers based on polyacrylamide. *Egypt J Pet* 27:897–910. <https://doi.org/10.1016/j.ejpe.2018.01.006>
21. Charitha BP, Rao P (2018) Pullulan as a potent green inhibitor for corrosion mitigation of aluminum composite: electrochemical and surface studies. *Int J Biol Macromol* 112:461–472. <https://doi.org/10.1016/j.ijbiomac.2018.01.218>
22. Obot IB, Onyechu IB, Kumar AM (2017) Sodium alginate: a promising biopolymer for corrosion protection of API X60 high strength carbon steel in saline medium. *Carbohydr Polym* 178:200–208. <https://doi.org/10.1016/j.carbpol.2017.09.049>
23. Saidi N, Elmsellem H, Ramdani M et al (2015) Using pectin extract as eco-friendly inhibitor for steel corrosion in 1M HCl media. *Der Pharma Chem* 7:87–94
24. Altwaiq A, mnim, Khouri SJ, Al-luaibi S, et al (2011) The role of extracted alkali lignin as corrosion inhibitor. *J Mater Environ Sci* 2:259–270. <https://doi.org/10.4197/Mar.23-2.5>

25. Wu W, Chen T, Du H et al (2016) Carboxymethyl starch as corrosion inhibitor for mild steel. *Emerg Mater Res* 5:277–283. <https://doi.org/10.1680/jemmr.15.00037>
26. Prabhu D, Padmalatha R (2013) Corrosion inhibition of 6063 aluminum alloy by *Coriandrum sativum* L seed extract in phosphoric acid medium. *J Mater Environ Sci* 4:732–743
27. Prabhu D, Rao P (2013) *Garcinia indica* as an environmentally safe corrosion inhibitor for aluminium in 0.5 M phosphoric acid. *Int J Corros*. <https://doi.org/10.1155/2013/945143>
28. B.P. C, Rao P, (2017) An ecofriendly approach for corrosion control of 6061 Al-15%(v) SiC(P) composite and its base alloy. *Chin J Chem Eng* 25:363–372. <https://doi.org/10.1016/j.cjche.2016.08.007>
29. Charitha BP, Chenan A, Rao P (2017) Enhancement of surface coating characteristics of epoxy resin by dextran: an electrochemical approach. *Ind Eng Chem Res* 56:1137–1147. <https://doi.org/10.1021/acs.iecr.6b03274>
30. Prakashaiah BG, Vinaya Kumara D, Anup Pandith A et al (2018) Corrosion inhibition of 2024–T3 aluminum alloy in 3.5% NaCl by thiosemicarbazone derivatives. *Corros Sci* 136:326–338. <https://doi.org/10.1016/j.corsci.2018.03.021>
31. Singh P, Ebenso EE, Olasunkanmi LO et al (2016) Electrochemical, theoretical, and surface morphological studies of corrosion inhibition effect of green naphthyridine derivatives on mild steel in hydrochloric acid. *J Phys Chem C* 120:3408–3419. <https://doi.org/10.1021/acs.jpcc.5b11901>
32. Verma C, Olasunkanmi LO, Ebenso EE et al (2016) Adsorption behavior of glucosamine-based, pyrimidine-fused heterocycles as green corrosion inhibitors for mild steel: experimental and theoretical studies. *J Phys Chem C* 120:11598–11611. <https://doi.org/10.1021/acs.jpcc.6b04429>
33. Ansari KR, Quraishi MA, Singh A et al (2016) Corrosion inhibition of N80 steel in 15% HCl by pyrazolone derivatives: electrochemical, surface and quantum chemical studies. *RSC Adv* 6:24130–24141. <https://doi.org/10.1039/c5ra25441h>
34. Bentiss F, Traisnel M, Lagrenee M (2000) The substituted 1,3,4-oxadiazoles: a new class of corrosion inhibitors of mild steel in acidic media. *Corros Sci* 42:127–146. [https://doi.org/10.1016/S0010-938X\(99\)00049-9](https://doi.org/10.1016/S0010-938X(99)00049-9)
35. Khadiri A, Saddik R, Bekkouche K et al (2016) Gravimetric, electrochemical and quantum chemical studies of some pyridazine derivatives as corrosion inhibitors for mild steel in 1 M HCl solution. *J Taiwan Inst Chem Eng* 58:552–564. <https://doi.org/10.1016/j.jtice.2015.06.031>
36. Abd El-Maksoud SA, Fouda AS (2005) Some pyridine derivatives as corrosion inhibitors for carbon steel in acidic medium. *Mater Chem Phys* 93:84–90. <https://doi.org/10.1016/j.matchemphys.2005.02.020>
37. Zhang XG (1996) *Corrosion and electrochemistry of Zinc*, 1st edn. Springer, New York
38. Li WH, He Q, Zhang ST et al (2008) Some new triazole derivatives as inhibitors for mild steel corrosion in acidic medium. *J Appl Electrochem* 38:289–295. <https://doi.org/10.1007/s10800-007-9437-7>
39. Zulfareen N, Venugopal T, Kannan K (2018) Experimental and theoretical studies on the corrosion inhibition of brass in hydrochloric acid by N-(4-(4-Benzhydryl Piperazin-1-yl) Methyl Carbamoyl) Phenyl) Furan-2-Carboxamide. *Int J Corros* 2018:1–18
40. Abdel-Gaber AM (2007) Effect of immersion time and temperature on the inhibition of the acid corrosion of zinc by fenugreek seeds extract. *Int J Appl Chem* 3:161–174
41. Manov S, Lamazouère AM, Ariès L (2000) Electrochemical study of the corrosion behaviour of zinc treated with a new organic chelating inhibitor. *Corros Sci* 42:1235–1248. [https://doi.org/10.1016/S0010-938X\(99\)00132-8](https://doi.org/10.1016/S0010-938X(99)00132-8)
42. Singh AK, Quraishi MA (2010) Effect of Cefazolin on the corrosion of mild steel in HCl solution. *Corros Sci* 52:152–160. <https://doi.org/10.1016/j.corsci.2009.08.050>
43. Oguzie EE, Njoku VO, Enenebeaku CK et al (2008) Effect of hexamethylpararosaniline chloride (crystal violet) on mild steel corrosion in acidic media. *Corros Sci* 50:3480–3486. <https://doi.org/10.1016/j.corsci.2008.09.017>
44. Bouklah M, Hammouti B, Lagrenée M, Bentiss F (2006) Thermodynamic properties of 2,5-bis(4-methoxyphenyl)-1,3,4-oxadiazole as a corrosion inhibitor for mild steel in normal sulfuric acid medium. *Corros Sci* 48:2831–2842. <https://doi.org/10.1016/j.corsci.2005.08.019>
45. Şahin M, Bilgiç S, Yilmaz H (2002) The inhibition effects of some cyclic nitrogen compounds on the corrosion of the steel in NaCl mediums. *Appl Surf Sci* 195:1–7. [https://doi.org/10.1016/S0169-4332\(01\)00783-8](https://doi.org/10.1016/S0169-4332(01)00783-8)
46. Nwosu FO, Muzakir MM (2016) Thermodynamic and adsorption studies of corrosion inhibition of mild steel using lignin from siam weed (*chromolaena odorata*) in acid medium. *J Mater Environ Sci* 7:1663–1673
47. Hebbar N, Praveen BM, Prasanna BM, Venkatesha TV (2015) Corrosion inhibition behaviour of ketosulfone for zinc in acidic medium. *J Fundam Appl Sci* 7:271–289
48. Biswas A, Pal S, Udayabhanu G (2015) Experimental and theoretical studies of xanthan gum and its graft co-polymer as corrosion inhibitor for mild steel in 15% HCl. *Appl Surf Sci* 353:173–183. <https://doi.org/10.1016/j.apsusc.2015.06.128>
49. Bentiss F, Traisnel M, Lagrenee M (2001) Influence of 2,5-bis(4-dimethylaminophenyl)-1,3,4-thiadiazole on corrosion inhibition of mild steel in acidic media. *J Appl Electrochem* 31:41–48
50. Hosseini M, Mertens SFL, Arshadi MR (2003) Synergism and antagonism in mild steel corrosion inhibition by sodium dodecylbenzenesulphonate and hexamethylenetetramine. *Corros Sci* 45:1473–1489. [https://doi.org/10.1016/S0010-938X\(02\)00246-9](https://doi.org/10.1016/S0010-938X(02)00246-9)
51. Okafor PC, Zheng Y (2009) Synergistic inhibition behaviour of methylbenzyl quaternary imidazoline derivative and iodide ions on mild steel in H₂SO₄ solutions. *Corros Sci* 51:850–859. <https://doi.org/10.1016/j.corsci.2009.01.027>
52. Quraishi MA, Rawat J, Ajmal M (2000) Dithiobiurets: a novel class of acid corrosion inhibitors for mild steel. *J Appl Electrochem* 30:745–751. <https://doi.org/10.1023/A:1004099412974>
53. Krishnaveni K, Sampath K, Ravichandran J, Jayabalakrishnan C (2015) N-methyl-2-(2-nitrobenzylidene) hydrazine carbthioamide—a new corrosion inhibitor for mild steel in 1 mol-L-1 hydrochloric acid. *Chinese J Chem Eng* 23:1916–1922. <https://doi.org/10.1016/j.cjche.2015.08.004>
54. Hu Q, Qiu Y, Zhang G, Guo X (2015) Capsella bursa-pastoris extract as an eco-friendly inhibitor on the corrosion of Q235 carbon steels in 1 mol-L- 1 hydrochloric acid. *Chin J Chem Eng* 23:1408–1415. <https://doi.org/10.1016/j.cjche.2015.05.002>
55. Mahida MB, Chaudhari HG (2012) Aliphatic amines as corrosion inhibitors for zinc in hydrochloric acid. *Der Pharma Chem* 4:2305–2312
56. Vashi RT, Desai K (2012) Hexamine as corrosion inhibitor for zinc in hydrochloric acid. *Der Pharma Chem* 4:2117–2123
57. Abboud Y, Abourriche A, Saffaj T et al (2009) A novel azo dye, 8-quinolinol-5-azoantipyrine as corrosion inhibitor for mild steel in acidic media. *Desalination* 237:175–189. <https://doi.org/10.1016/j.desal.2007.12.031>
58. Benabdellah M, Yahyi A, Dafali A et al (2011) Corrosion inhibition of steel in molar HCl by triphenyltin-2-thiophene carboxylate. *Arab J Chem* 4:243–247. <https://doi.org/10.1016/j.arabj.2010.06.055>
59. Dahiya S, Kumar P, Lata S et al (2017) An exhaustive study of a coupling reagent (1-(3-dimethylaminopropyl) 3-ethylcarbodiimide

- hydrochloride) as corrosion inhibitor for steel. *Indian J Chem Technol* 24:327–335
60. Gupta NK, Verma C, Salghi R et al (2017) New phosphonate based corrosion inhibitors for mild steel in hydrochloric acid useful for industrial pickling processes: experimental and theoretical approach. *New J Chem* 41:13114–13129. <https://doi.org/10.1039/c7nj01431g>
61. Arukalam IO (2014) Durability and synergistic effects of KI on the acid corrosion inhibition of mild steel by hydroxypropyl methylcellulose. *Carbohydr Polym* 112:291–299. <https://doi.org/10.1016/j.carbpol.2014.05.071>
62. Idir B, Kellou-Kerkouche F (2018) Experimental and theoretical studies on corrosion inhibition performance of phenanthroline for cast iron in acid solution. *J Electrochem Sci Technol* 9:260–275
63. Chauhan DS, Ansari KR, Sorour AA et al (2018) Thiosemicarbazide and thiocarbohydrazide functionalized chitosan as eco-friendly corrosion inhibitors for carbon steel in hydrochloric acid solution. *Int J Biol Macromol* 107:1747–1757. <https://doi.org/10.1016/j.ijbiomac.2017.10.050>
64. Obot IB, Ebenso EE, Kabanda MM (2013) Metronidazole as environmentally safe corrosion inhibitor for mild steel in 0.5 M HCl: experimental and theoretical investigation. *J Environ Chem Eng* 1:431–439. <https://doi.org/10.1016/j.jece.2013.06.007>
65. Geerlings P, De Proft F, Langenaeker W (2003) Conceptual density functional theory. *Chem Rev* 103:1793–1873. <https://doi.org/10.1021/cr990029p>
66. Obot IB, Macdonald DD, Gasem ZM (2015) Density functional theory (DFT) as a powerful tool for designing new organic corrosion inhibitors: Part 1: an overview. *Corros Sci* 99:1–30. <https://doi.org/10.1016/j.corsci.2015.01.037>
67. Gao G, Liang C (2007) Electrochemical and DFT studies of β -amino-alcohols as corrosion inhibitors for brass. *Electrochim Acta* 52:4554–4559. <https://doi.org/10.1016/j.electacta.2006.12.058>
68. Hasanov R, Sadikoğlu M, Bilgiç S (2007) Electrochemical and quantum chemical studies of some Schiff bases on the corrosion of steel in H_2SO_4 solution. *Appl Surf Sci* 253:3913–3921. <https://doi.org/10.1016/j.apsusc.2006.08.025>
69. Li W, He Q, Pei C, Hou B (2007) Experimental and theoretical investigation of the adsorption behaviour of new triazole derivatives as inhibitors for mild steel corrosion in acid media. *Electrochim Acta* 52:6386–6394. <https://doi.org/10.1016/j.electacta.2007.04.077>

Publisher's Note Springer Nature remains neutral with regard to jurisdictional claims in published maps and institutional affiliations.